P2.29 **A CLIMATOLOGICAL STUDY OF ICE CLOUD REFLECTIVITY**

Daniel T. Lindsey*
NOAA/NESDIS/ORA/RAMMB
Fort Collins, Colorado

1. INTRODUCTION

Satellite observations of thunderstorms have been widely documented since the launch of Geostationary Operational Environmental Satellites (GOES) in the 1970's. The current generation of GOES satellites have several added capabilities, including the addition of a channel centered near 3.9 μm, within the shortwave infrared portion of the electromagnetic spectrum. During the daytime, satellite-observed radiances at this channel include an emitted thermal component and a reflected solar component. For sufficiently optically thick clouds, the thermal component can be approximated by assuming the emitting temperature is the same at 3.9 μm as at 10.7 μm (GOES channel 4). Given observed 3.9 μm radiance, it is then possible to calculate the 3.9 μm solar reflected component. This is often represented as an albedo, or the percent of incoming solar radiation at 3.9 μm which is reflected back to the satellite.

Setvák and Doswell (1991) first noted, using advanced very high resolution radiometer (AVHRR) data, that some thunderstorm tops have enhanced solar reflectivity in the shortwave infrared portion of the spectrum. They suggest that differences in 3.9 μm albedo may be due to differences in microphysical structure at cloud-top. It is well documented that liquid water clouds are more effective reflectors than ice clouds (e.g., Turk et al. 1998). However, thunderstorm tops often exist at temperatures well below -40 ˚C, meaning their composition is dominated by ice crystals. Differences in the size distributions of these ice crystals have an effect on shortwave infrared reflectivity: research has shown that more numerous smaller crystals tend to be more effective reflectors (Melani et al. 2003a,b). As a result, satellite detection of a "reflective" thunderstorm top implies that its anvil is composed of relatively small and numerous ice crystals, and this may provide information about internal thunderstorm structure (Setvák et al. 2003).

Examples of thunderstorms with relatively high and low 3.9 μm albedo are given in Figures 1a and 1b, respectively. Both of these days resulted in significant severe weather. Values of 3.9 μm albedo for storms in Fig. 1a approach 15%, while values in Fig. 1b are generally less than 5%.

*Corresponding author address: Daniel T. Lindsey, CIRA/Colorado State University, 1375 Campus Delivery, Ft. Collins, CO 80523-1375; email: lindsey@cira.colostate.edu

a)

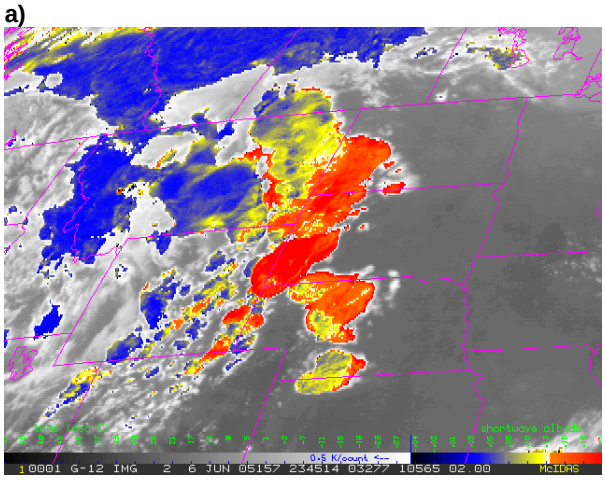

b)

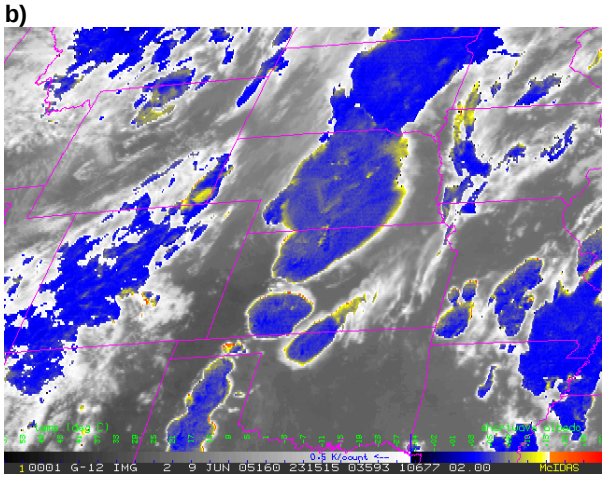

Figure 1. GOES-12 channel 4 (10.7 μm) for brightness temperatures greater than -30˚ C, and 3.9 μm albedo for brightess temperatures less than -30˚ C (colors), for a) 6 June 2005 at 2345 UTC, and b) 9 June 2005 at 2315 UTC. Warmer colors indicate cold cloud tops with relatively large 3.9 μm albedo values.

The primary goals of this study are to look at this reflective thunderstorm top phenomenon from a climatological perspective and seek mechanisms for the existence of small ice at cloud top. An explanation for significant differences in cloud-top 3.9 μm albedo between two storms (as in Fig. 1) is sought. Section 2 will describe a climatological study of reflective ice clouds over the US; section 3 presents results of a statistical study using reanalysis data; section 4

presents a possible physical mechanism; section 5 offers a summary and areas for future work.

2. REFLECTIVE ICE CLOUD CLIMATOLOGY

GOES-West (GOES-10) and GOES-East (GOES-8 and GOES-12) data were analyzed every 2 hours from 2000, 2003, and 2004. Channel 4 (10.7 μm) and channel 2 (3.9 μm) radiances were used to calculate the 3.9 μm albedo at every pixel within the domain for the entire year. Only times when the solar zenith angle was less than 68˚ were included, since the albedo calculation has large errors near sunrise and sunset, and is impossible at night. The analysis was also limited to cloudy pixels with 10.7 μm brightness temperatures colder than -40˚ C. This was an attempt to eliminate thin cirrus, and ensured that the clouds were composed almost entirely of ice crystals (no liquid water droplets).

Figure 2a shows the results of the climatological study from GOES-East. Contours represent the mean 3.9 μm albedo of ice clouds (defined above). This quantity was calculated following the method outlined by Setvák and Doswell (1991). Pixels were grouped into 1x1 degree (lat/lon) boxes before the means were computed. The maximum over the high plains and moutainous regions is obvious. Areas east of ~100˚ W longitude have values near 2%, while values in eastern Colorado exceed 5.5%. Figure 2b is similar to Fig. 2a, except for the GOES-West domain. Values throughout the west are larger, and maxima are evident in eastern Colorado, northwest Montana, and southeast California. These areas are all downwind of major mountain ranges, suggesting that high terrain may play an important role in the mechanism for generating highly reflective clouds. Values over eastern Colorado are slightly smaller from the GOES-West perspective compared to those from GOES-East (Fig. 2a). This is likely due to preferential forward scattering when the sun is approaching the western horizon and the convective activity reaches a maximum in late afternoon.

Figures 3a and 3b show the same data from a slightly different perspective. Here, the percent of ice cloud pixels whose 3.9 μm albedo is greater than 5% are contoured. The choice of the 5% threshold was arbitrary; changing the threshold had a negligible effect on the resulting geographical distribution. Note that over the high plains over 40% of ice clouds have greater than 5% 3.9 μm albedo, while further east, less than 5% exceed this threshold. This, along with a more thorough analysis of distributions about the mean, shows that albedos greater than 5% are rare in the east. In the longitudinal band between 110˚W-100˚W, values greater than 5% are quite common, and albedos greater than 10% are not infrequent.

a)

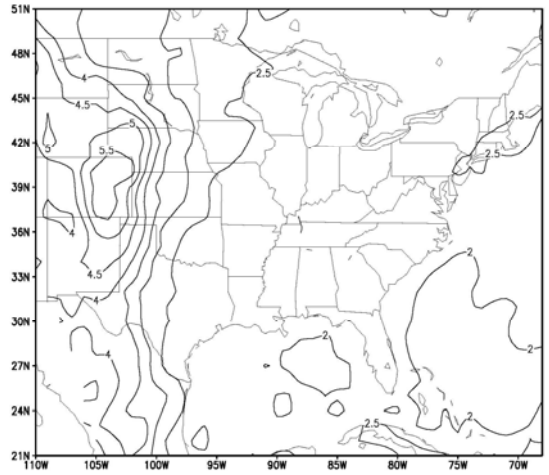

b)

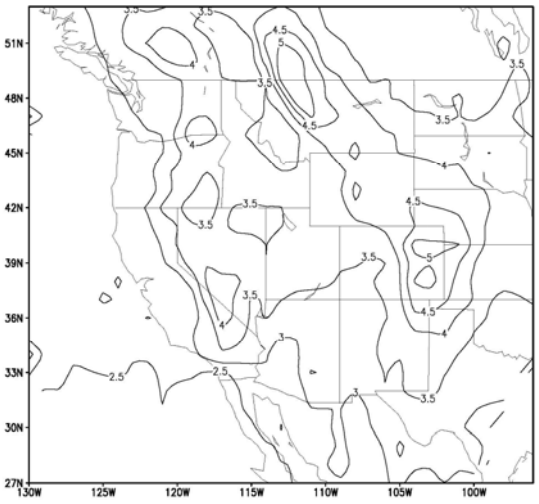

Figure 2. Mean 3.9 μm albedo of ice clouds from GOES-East (a) and GOES-West (b), from 2000, 2003, and 2004, for times when the solar zenith angle is less than 68˚.

Analysis of the monthly trend of reflective tops for the longitudinal band between 105W - 95W (Fig. 4a,b) reveals a maximum during the summer months and a secondary maximum during the winter, with minima in the fall and spring. The summertime maximum is primarily associated with convection, while the secondary winter maximum is primarily associated with mountain wave clouds, which also tend to be relatively reflective. Ice clouds with 3.9 μm albedos greater than 5% east of 95W are quite rare, especially during the summer (Fig. 4a). The western part of the continental US has more reflective ice clouds on average (see also Fig. 3b). The band between 105W - 95W shows the same trend with GOES-West as with GOES-East, while the bands further west have more complex month-to-

month variability. Current thinking is that the western maxima are dominated by mountain wave clouds, since the maxima lie at or just downstream of major mountain ranges (Fig. 3b). The multiple peaks in the western U.S. longitudinal bands may be dominated by noise, since ice cloud frequency is quite low during certain months.

a)

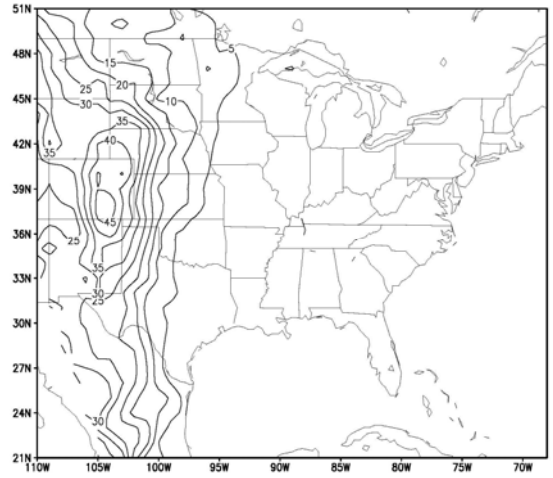

b)

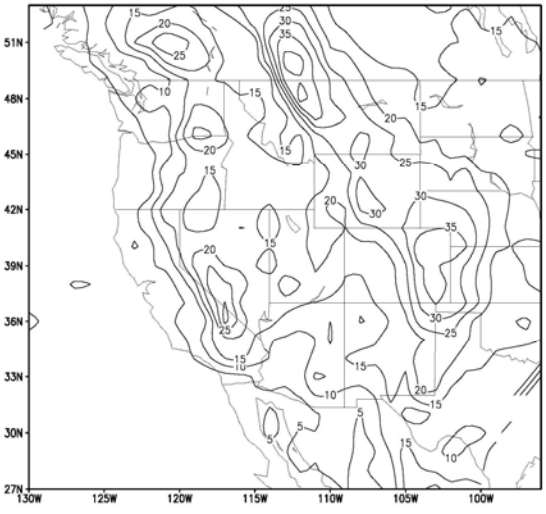

Figure 3. Percent of ice clouds whose 3.9 μm albedo exceeds 5% from a) GOES-East and b) GOES-West, from 2000, 2003, and 2004, for times when the solar zenith angle is less than 68˚.

a)

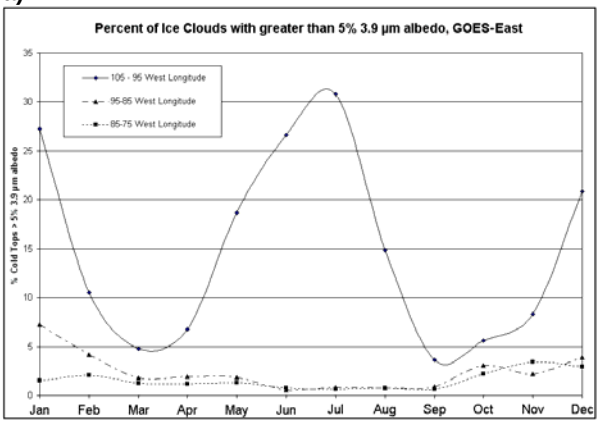

b)

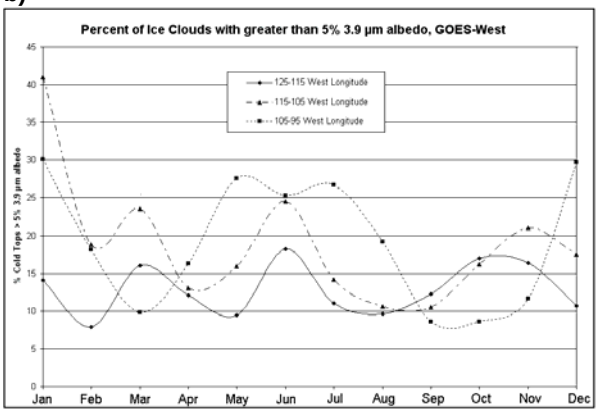

Figure 4. Monthly distribution of percent of ice cloud pixels exceeding 5% 3.9 μm albedo, divided into longitudinal bands, for a) GOES-East and b) GOES-West.

In order to isolate ice clouds associated with convection, the same analysis as in Fig. 2 was applied only during May, June, July, and August, and the results are plotted in Figs. 5a and 5b. Mean 3.9 μm albedo values are even greater during the summer months than the entire year over the mountains and high plains. This suggests that thunderstorms generate more reflective anvils than other ice clouds (like mountain wave clouds and thick cirrus). It's also interesting that the gradient in western Kansas appears greater from GOES-East compared to GOES-West. This shows that forward scattering is favored. In eastern Colorado, convective activity peaks in the late afternoon, so GOES-East is in a position to measure more forward-scattered radiation. In central and eastern Kansas, a significant peak in ice cloud frequency occurs in the morning, so that GOES-West detects radiation scattered in the forward direction. The end result is an apparent tighter gradient as viewed from GOES-East.

a)

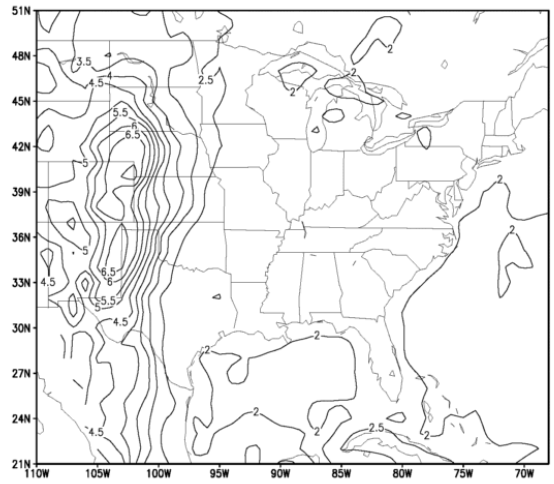

b)

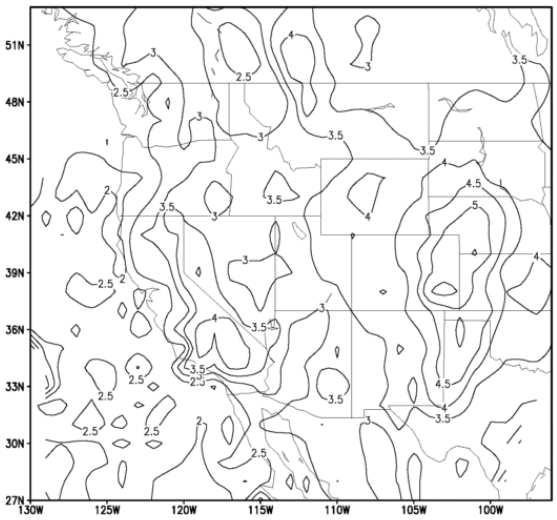

Figure 5. Same as Fig. 2, except only for May, June, July, and August.

3. STATISTICAL ANALYSIS

In an effort to understand the physical basis behind the geographical signal in the climatological figures above, a statistical method was applied to several theromdynamic parameters in the following way. First, a domain was chosen from Fig. 2a roughly within the 4.5% contour, or between approximately 30˚-45˚ N. latitude and between 100˚-110˚ W. longitude. Satellite data during the summer months (June, July, August) of 2003 and 2004 were analyzed, and 16 convective days having a large percentage of reflective thunderstorm tops (hereafter referred to as "reflective days") and 16 convective days having a low percentage of reflective thunderstorm tops ("non-reflective days") were selected. Though not used in this particular analysis, days similar to those in Figures 1a and 1b are typical examples of a reflective day and a non-reflective day, respectively.

For each of the 16 reflective and 16 non-reflective days, grid points from the North American Regional Reanalysis (NARR) dataset falling within an area containing the convective clouds were selected. NARR data is similar to the NCEP/NCAR reanalysis, but includes data from more sources. Additionally, grid spacing is 32-km, so between 500 and 1000 grid points were available for each day, depending on the size of box chosen. Grid point values at 0000 UTC of temperature, dewpoint, and wind from the surface to 100 mb were averaged for each of the 16 days. These mean profiles were then averaged for the reflective days and non-reflective days, producing two final mean profiles. These are given in Figure 6.

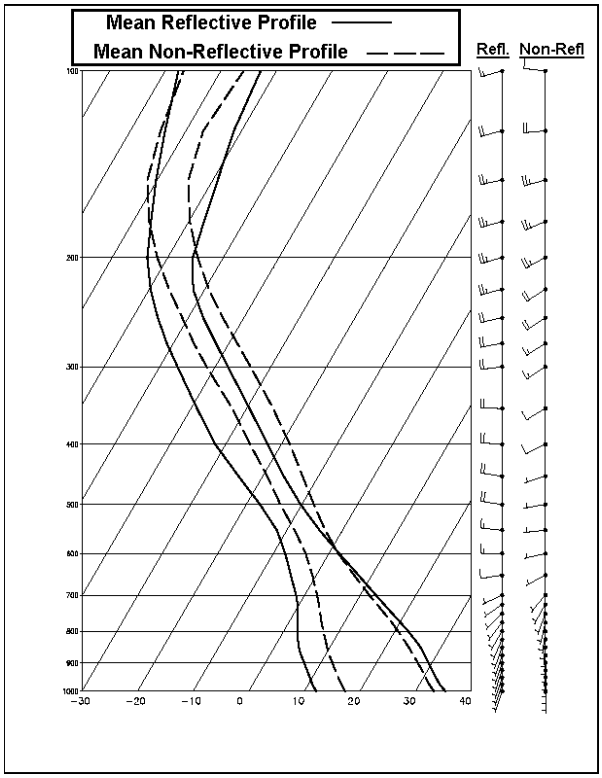

Figure 6. Mean temperature (right) and dewpoint (left) profiles for the reflective (solid) and non-reflective (dashed) cases, along with mean wind profiles, plotted on a traditional skew-T/log-p diagram. A full wind barb represents 10 knots.

There are several important differences between these two mean profiles. First, the relative humidity throughout the reflective profile is lower, especially in the lowest 400 mb. A larger temperature/dewpoint spread near the surface suggests a fairly dry boundary layer is supportive of reflective thunderstorm tops. (This can also be inferred by looking at the climatology maps in Figure 2). Secondly, and possibly more importantly, the 800-300 mb lapse rate is noticeably

steeper in the reflective case. This environment would promote more instability and stronger updrafts. Finally, the mid-level westerlies are stronger in the reflective case.

To get a more quantitative understanding of the results, values of several variables were collected at each grid point, and means and standard deviations were calculated for each of the 32 days. Next, the resulting means were averaged together for each case (reflective and non-reflective), and the standard deviations were also averaged. Results are given in Table 1. To estimate significance, a difference of means t-test was performed, using the mean standard deviations calculated above. Variables in Table 1 with greater than 95% significance are shaded in light gray; those exceeding 99% significance are shaded in dark gray. It should be noted that standard deviations were also calculated for the daily distributions of means (as opposed to the grid point mean for each day), and these were lower than the average standard deviations, so the larger, more conservative estimates were used.

	Reflective Case Mean	Non-Reflective Case Mean
CAPE (J/kg)	567	219
Precipitable Water (mm)	17.7	23.1
Surface Temperature (˚C)	28.2	26.1
Surface Dew Point (˚C)	4.5	7.2
700 hPa RH (%)	42	56
500 hPa RH (%)	58	65
800-500 hPa Lapse Rate (˚C per km)	8.5	7.4
Sfc - 500 hPa Zonal Shear (ms^{-1})	9.9	2.3
Depth of cloud base to -38 ˚C level (m)	5210	6036

Table 1. Means for several variables for the 16 reflective days and 16 non-reflective days. Light gray shading indicates the difference of means exceeds 95% significance; dark gray for difference of means exceeding 99% significance.

The CAPE for the reflective case is over twice that of the non-reflective case, verifying that instability is greater in the reflective situation (even though convection was observed in both cases). Precipitable water values are smaller and 700mb relative humidity values are lower for the reflective case, further underscoring the possible importance of relatively dry air. Lapse rates are significantly steeper in the reflective case (the standard deviations for lapse rate were very small), and the surface-to-500-mb zonal shear is much larger on reflective days. Surface temperature and dewpoint values were used to calculate the lifted condensation level (LCL). Using this as the cloud base height, the distance from cloud base to the homogeneous freezing level, taken to be -38 ˚C, was calculated for both cases, and cloud depths are significantly larger in the non-reflective case. The explanation behind choosing the depth from the LCL to -38 ˚C is below.

4. POSSIBLE PHYSICAL MECHANISM

Before proposing a physical mechanism to explain variations in thunderstorm top 3.9 μm albedo, it is necessary to establish a link between satellite-measured reflectivity and the cloud-top ice crystal distribution. To do this, an observational operator is employed to compute expected GOES radiance values from a user-controlled ice cloud. For details of the observational operator, see Greenwald et al. (2002). A cloud composed of pristine ice was placed at 12-km AGL, near the tropopause, and the thickness was set to 2-km. Mass mixing ratio and number concentration were then varied to produce a range of ice crystal mean diameters for an assumed Gamma size distribution; for each mean diameter, the 3.9 μm albedo was calculated, and the results are plotted in Figure 7.

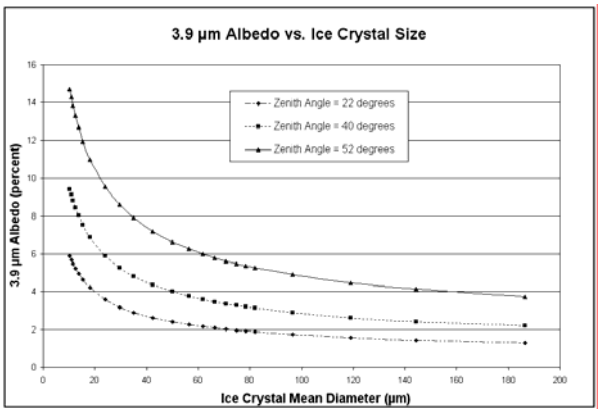

Figure 7. Model results for 2-km-thick cloud composed of pristine ice, for 3 solar zenith angles.

For a given solar zenith angle, the 3.9 μm albedo is fairly insensitive to ice crystal size for diameters greater than about 80 μm, but for smaller values, the 3.9 μm albedo increases. According to the model, increasing the solar zenith angle (as the sun approaches the horizon) also produces an increase in 3.9 μm albedo for a given ice crystal size distribution. The important result is that ice crystal cloud reflectivity increases dramatically for small ice crystal sizes. It should also be noted that the model predicted 10.7 μm brightness temperatures near 220 K (approximately the tropopause temperature) for all ice crystal sizes. This means that the cloud was sufficiently optically thick to prevent any emitted terrestrial radiation from penetrating it.

If a large number of small ice crystals is indeed the source of ice clouds with enhanced 3.9 μm albedo, the next logical question becomes, "Why do some cloud tops have smaller ice crystals than others?" Results from Section 3 show that in the high plains during the summer months, certain thermodynamic environments favor thunderstorms with smaller ice crystals, but this offers little evidence into the physical mechanism leading to small ice production. Rosenfeld and Lensky (1998) discuss differences between microphysical profiles in maritime and continental clouds. Continental clouds have a deeper diffusional droplet growth zone than maritime clouds, so that continental cloud droplets

forming near cloud base grow very slowly with depth as they ascend within the updraft. This effect is exaggerated as updraft magnitudes increase. Collision-coalescence efficiency decreases as cloud droplet size decreases, so these droplets remain relatively small even at temperatures well below freezing. Heymsfield et al. (2005) use aircraft measurements during CRYSTAL-FACE along with a 1D parcel model to study the effects of homogeneous ice nucleation in clouds with varying properties, including depth and updraft velocity. Their Figs. 13 and 16 show that stronger updrafts support larger supersaturation with respect to liquid water, which prevents the smallest droplets from evaporating before freezing homogeneously. Additionally, parcels initiated at colder temperatures produce smaller droplets and therefore smaller ice crystals. Their Fig. 14 shows that clouds whose cloud-base temperature is warmer (lower in altitude) produce significantly larger mean droplet diameters just prior to the onset of homogeneous ice nucleation, because droplets have a longer time to grow. These two studies suggest that, in general, the anvils of high-based clouds with strong updrafts contain smaller and more numerous ice crystals.

In order to test this hypothesis with satellite and NARR data, GOES-East data over all of the eastern U.S. from 2145 UTC on each of the 32 days described in Section 4 (during the summer) were analyzed to select 978 individual clouds having at least 50 pixels with 10.7 μm brightness temperatures colder than -40 ˚C. For each cloud, the mean 3.9 μm albedo was calculated, and the nearest NARR grid point from 2100 UTC was selected. In order to eliminate non-convective environments in the NARR data, only grid points whose mean-layer CAPE exceeded 200 J kg^{-1} and whose cloud depth between the LCL and the -38 ˚C level exceeded 1 km were allowed. Since

$$w_{\max} = \sqrt{2CAPE}\,, \qquad (1)$$

where $w_{\max}$ is the maximum possible vertical velocity, we define a quantity called the cloud droplet residence time (τ) as

$$\tau = \frac{D_{LCL/-38}}{w_{\max}}\,, \qquad (2)$$

where $D_{LCL/-38}$ is the depth from the LCL to the -38 ˚C level. The cloud droplet residence time is a rough estimate of how long a cloud droplet which formed at cloud base exists within the updraft before reaching the -38 ˚C level, and is therefore a function of both cloud depth and updraft velocity. Figure 8 shows the mean 3.9 μm albedo of each cloud plotted against the NARR-derived residence time. Those 3.9 μm albedo values exceeding 5% were limited almost entirely to droplet residence times less than 100 s; in other words, if a cloud droplet population remains below the homogeneous freezing level too long, its mean diameter will increase and its number concentration will decrease sufficiently to prevent significant reflection of incoming 3.9 μm radiation. The variance about a best-fit curve through the points in Fig. 6 could be explained by any of the following: 1) additional mechanisms, such as entrainment and CCN distributions, may play a role in anvil ice crystal properties, 2) errors in the NARR dataset, especially with the CAPE and surface temperature and moisture values matching the true environment in which each cloud forms, 3) 3.9 μm albedo is a function of more than just ice crystal mean diameter, and 4) GOES footprint is large, so 3.9 μm albedo measurements may not properly represent the actual cloud properties. If the variance is dominated by 2), one could theoretically measure the 3.9 μm albedo of a glaciated cloud, use nearby surface and sounding data to estimate the residence time, then compare the observed albedo value to the predicted value from the best-fit in Fig. 6. Observed albedos larger than the predicted value suggest that the sounding-observed CAPE is too low, and the actual updraft within the cloud is stronger than expected. In this way, 3.9 μm albedo may be used as a thunderstorm nowcasting tool to infer updraft strength. Further research is required to determine whether this method is practical. This physical mechanism is consistent with the climatological results in Figs. 2 and 3. Thunderstorms forming in the mountains and high plains tend to have relatively high bases, due to dry boundary layers and elevated terrain. The largest 3.9 μm albedo values in Figs. 2 and 3 occur just east of the Rocky Mountains, a region which will have both high cloud bases and fairly strong updrafts.

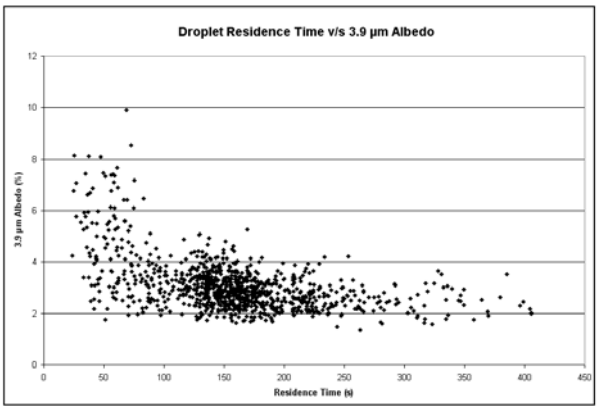

Figure 8. Mean 3.9 μm albedo plotted against cloud droplet residence time (seconds) between the lifted condensation level and the -38 ˚C level. This quantity is estimated by dividing the cloud depth by the square root of twice the CAPE.

Until now, the discussion has been limited to thunderstorm anvil clouds. As discussed in Section 2, observations reveal that mountain wave clouds tend to have large 3.9 μm albedo values. This is consistent with results from Heymsfield and Miloshevich (1993), where it is found that ice crystals in mountain wave clouds form primarily by homogeneous nucleation and

tend to be quite small (mean diameters in the 10-20 μm range). If all wave clouds have similar characteristics to those in the study, one might expect them to exhibit large 3.9 μm albedo values, assuming the validity of the model calculations shown in Fig. 5.

5. SUMMARY AND FUTURE WORK

This study examines the reflectivity of thunderstorm tops as measured from the GOES 3.9 μm channel. A climatological analysis reveals that environmental conditions in mountainous regions of the U.S. favor storms with enhanced 3.9 μm albedo, while storm-top reflectivity over much of the eastern U.S. is lower. Model results show that these storm-top 3.9 μm albedo differences are due to variations in ice crystal size and number concentration; smaller ice crystal distribution mean diameters result in larger 3.9 μm albedo. Reanalysis data is used to show that highly reflective thunderstorms tend to occur in environments with relatively dry boundary layers, steep lapse rates, large vertical shear, and small distances from cloud base to the homogeneous freezing level. A physical mechanism, called the cloud droplet residence time, is presented which explains why storms in mountainous areas have larger mean 3.9 μm albedos. If proven to be valid, thunderstorm updraft strength information can be obtained from GOES 3.9 μm albedo measurements.

Setvák et al. (2003) discuss observations of thunderstorms with highly reflective plumes which appear to be ejected from a thunderstorm's overshooting top; the authors have made similar observations. If a thunderstorm with fairly uniform 3.9 μm albedo values suddenly begins ejecting smaller ice crystals from its updraft, results of this study suggest that its updraft may have recently strengthened, allowing more tiny cloud droplets to freeze homogeneously (instead of evaporating, perhaps). This observation also has potential nowcasting applications.

Work is currently underway to improve the model simulations presented in Section 3. We plan to use more sophisticated ways of representing the scattering phase function, along with allowing ice crystal habit to vary. The eventual goal is to obtain an accurate relationship between 3.9 μm albedo and ice crystal size and habit, so that satellite measurements of 3.9 μm albedo may provide information about cloud-top microphysical structure. In addition, satellite measurements from other platforms, such as the Moderate Resolution Imaging Spectroradiometer (MODIS) instrument aboard the polar-orbiting satellites Terra and Aqua, may provide independent estimates of ice crystal size to validate our model simulations.

7. ACKNOWLEDGEMENTS

This research was supported by NOAA Grant NA17RJ1228. The views, opinions, and findings in this report are those of the author, and should not be construed as an official NOAA and or U.S. Government position, policy, or decision.

8. REFERENCES

Greenwald, T. J., R. Hertenstein, and T. Vukićević, 2002: An all-weather observational operator for radiance data assimilation with mesoscale forecast models. *Mon. Wea. Rev.*, **130**, 1882-1897.

Heymsfield, A. J., and L. M. Miloshevich, 1993: Homogeneous ice nucleation and supercooled liquid water in orographic wave clouds. *J. Atmos. Sci.*, **50**, 2335-2353.

———, L. M. Miloshevich, C. Schmitt, A. Bansemer, C. Twohy, M. R. Poellot, A. Fridlind, and H. Gerber, 2005: Homogeneous ice nucleation in subtropical and tropical convection and its influence on cirrus anvil microphysics. *J. Atmos. Sci.*, **62**, 41-64.

Melani, S., E. Cattani, V. Levizzani, M. Cervino, and F. Torricella, 2003: Radiative effects of simulated cirrus clouds on top of a deep convective storm in METEOSAT second generation SEVIRI channels. *Meteorol. Atmos. Phys.*, **83**, 109-122.

———, E. Cattani, F. Torricella, and V. Levizzani, 2003: Characterization of plumes on top of a deep convective storm using AVHRR imagery and radiative transfer model simulations. *Atmos. Res.*, **67-68**, 485-499.

Rosenfeld, D., and I. M. Lensky, 1998: Satellite–based insights into precipitation formation processes in continental and maritime convective clouds. *Bull. Amer. Metero. Soc.*, **79**, 2457-2476.

Setvák, M., and C. A. Doswell III, 1991: The AVHRR channel 3 cloud top reflectivity of convective storms. *Mon. Wea. Rev.*, **119**, 841-847.

————, R. M. Rabin, C. A. Doswell III, V. Levizzani, 2003: Satellite observations of convective storm tops in the 1.6, 3.7, and 3.9 μm spectral bands. *Atmos. Res.*, **66-67,** 607-627.

Turk, J., J. Vivekanandan, T. Lee, P. Durkee, and K. Nielsen, 1998: Derivation and applications of near-infrared cloud reflectances from GOES-8 and GOES-9. *J. Appl. Meteor.*, **37**, 819-831.